SAND2020-8972C

Model Predictive Integrated Voltage and Frequency Support in Microgrids

Niranjan Bhujel†,
Timothy M. Hansen, and Reinaldo Tonkoski
South Dakota State University
Brookings, South Dakota, USA
Email: †niranjan.bhujel@jacks.sdstate.edu

Ujjwol Tamrakar, and Raymond H. Byrne
Sandia National Laboratories
Albuquerque, New Mexico, USA

***Abstract*—For the optimal performance of a microgrid where line resistance to reactance ($\mathbf{R/X}$) ratio is high, one must consider the coupling between voltage and frequency. Furthermore, microgrid operational costs are time-varying. Thus, the voltage and frequency support controller must be flexible enough to handle technical and economic constraints. In this paper, the model predictive control (MPC) approach is proposed for voltage and frequency support considering the coupling between voltage and frequency dynamics. With the predictive model of the system, the finite horizon optimization problem is solved online and a control signal is calculated such that defined cost is minimized. By proper choice of MPC parameters, desired performance based on the availability of resources and market incentives can be achieved.**

***Index Terms*—Voltage-frequency control, voltage-frequency coupling, model predictive control, optimal control, microgrid.**

I. Introduction

Microgrids have been proposed as a solution to achieve reliable and resilient grids of the future [1]. In isolated/islanded microgrids, synchronous generators are often responsible for maintaining the voltage and frequency of the system. The distributed energy resources (DERs), such as solar and energy storage systems (ESSs), typically act as passive elements or might have a secondary supporting role regarding voltage and frequency control. The large-scale integration of renewable DERs brings various challenges regarding dynamic voltage and frequency control. Microgrids have intrinsic differences compared to traditional interconnected power systems in terms of size, feeder type, high cross-coupling between voltage and frequency dynamics, a high share of converter-based renewable sources, and low-inertia [2], [3]. Further, microgrids operating in isolated/islanded mode are starting to become more common in distribution networks. In an isolated/islanded mode of operation, the primary controller is responsible for maintaining the voltage and frequency of the system. The loss of a single generator, inverter, or load, without proper coordination, can cause significant power imbalance and lead to large voltage and frequency deviations that compromise power quality and reliability. Thus, improved control techniques for DERs are required to maintain proper operation.

Traditionally, the voltage and frequency controllers are designed independently under the assumption that the voltage and frequency dynamics of the system are decoupled [4]. However, microgrids are typically operated at low to medium voltage ranges, hence the R/X ratio is typically very high [3]. Furthermore, changes in the system voltage will also be reflected as changes in the system load owing to the relatively small size of the microgrid. All these factors contribute to a stronger coupling between voltage and frequency dynamics in microgrids as compared to traditional grids. For combined voltage and frequency control, droop-based controllers have been traditionally used [5]. In this approach, the d and q components of the current are used to support the frequency and voltage, respectively, as a proxy for active and reactive power support. In general, droop-based approaches assume that voltage and frequency dynamics are decoupled. Another proposed method is to utilize voltage dependency of active power to control frequency [6]. In this method, voltage is modulated to regulate the frequency, but this does not work when majority of load power is insensitive to voltage deviations. Furthermore, a voltage-based frequency controller often conflicts or interferes with a voltage controller, making it difficult to achieve both control goals simultaneously.

The main objective of this paper is to present the formulation of an advanced predictive control framework for coordinating ESSs to provide voltage and frequency support considering voltage and frequency cross-coupling. Dynamic voltage and frequency support are power-intensive applications and can have significant impact on ESS degradation. Traditional controllers do not provide the flexibility to incorporate operating costs of ESSs (e.g., ESS lifetime degradation cost, impact on stacked services, energy cost) required to provide adequate voltage and frequency support. In this regard, a model predictive control (MPC)-based approach is proposed to handle the non-linear system voltage-frequency dynamics. Furthermore, this approach provides the flexibility to tune controller performance and incorporate operational constraints within the formulation. MPC-based approaches have been previously proposed in [7]–[9] under the assumption that the voltage and frequency dynamics are decoupled. The pro-

This work is partially supported by the National Science Foundation (NSF) grant MRI-1726964. This research made use of the "Roaring Thunder" cluster at South Dakota State University funded under NSF grant number CNS-01726946 and OAC-1924302.

The authors would like to thank Dr. Imre Gyuk, Director of Energy Storage Research, Office of Electricity for his funding and guidance on this research.

978-1-7281-8192-9/21/$31.00 ©2021 IEEE.

posed framework addresses the technical challenges associated with low inertia, fast voltage dynamics, cross-coupling, and coordination of voltage and frequency controls, which can cause local power quality issues (e.g., voltage deviations, sympathetic over/under voltages, stability issues, outages, or large-area blackouts).

The paper is organized as follows: Section II develops a model for integrated voltage and frequency dynamics of an isolated power system. In Section III, a MPC approach is presented and the time constants for the voltage and frequency dynamics are derived. The proposed methodology is summarized in Section IV. The results and the findings are reviewed in Section V, and Section VI concludes the paper.

II. Dynamic Models for Microgrids

In this section, the voltage and frequency dynamics of the system are first independently modeled, and then a combined model is derived illustrating the cross-coupling between the voltage and frequency dynamics.

A. Voltage Dynamics Model

A single line diagram of an inverter-based ESS connected to a microgrid is shown in Fig. 1. The inverter is modeled as an average model of a current-controlled voltage source inverter (CC-VSI) while the grid is modeled by the Thevenin equivalent voltage v_g, and equivalent resistance and inductance R and L, respectively. At the point of common coupling (PCC), a capacitor C is added, which is part of the inverter filter (the inductor of the inverter filter is not shown because a voltage source and an inductor form a current source). The voltage across the capacitor is represented by v_c. The system load is also connected at the PCC, which draws current i_L.

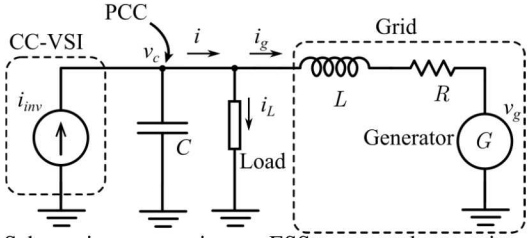

Fig. 1: Schematic representing an ESS connected to a microgrid.

The grid current i_g and capacitor voltage v_c can be described in the abc frame as:

$$\frac{di_{g,abc}}{dt} = \frac{v_{c,abc} - v_{g,abc} - i_{g,abc}R}{L} \tag{1}$$

$$\frac{dv_{c,abc}}{dt} = \frac{i_{inv,abc} - i_{g,abc} - i_{L,abc}}{C} \tag{2}$$

Applying Park's transformation and neglecting the zero component assuming a balanced system, the state-space representation of the system's voltage dynamics i_g and v_c in $dq0$ frame is given by:

$$\dot{x}_v = A_v x_v + B_v u_v \tag{3}$$

with

$$A_v = \begin{bmatrix} -\frac{R}{L} & \omega & \frac{1}{L} & 0 \\ -\omega & -\frac{R}{L} & 0 & \frac{1}{L} \\ -\frac{1}{C} & 0 & 0 & \omega \\ 0 & -\frac{1}{C} & -\omega & 0 \end{bmatrix} \tag{4}$$

$$B_v = \begin{bmatrix} -\frac{1}{L} & 0 & 0 & 0 & 0 & 0 \\ 0 & -\frac{1}{L} & 0 & 0 & 0 & 0 \\ 0 & 0 & \frac{1}{C} & 0 & -\frac{1}{C} & 0 \\ 0 & 0 & 0 & \frac{1}{C} & 0 & -\frac{1}{C} \end{bmatrix} \tag{5}$$

where $x_v = [i_{gd}\ i_{gq}\ v_{cd}\ v_{cq}]^\top$ is the state vector representing the voltage dynamics of the system, and $u_v = [v_{gd}\ v_{gq}\ i_{invd}\ i_{invq}\ i_{Ld}\ i_{Lq}]^\top$ represents the inputs.

It is important to note that the synchronous generator's voltage dynamics with respect to frequency deviations have not been considered because v_g is estimated through a feedforward term.

B. Frequency Dynamics Model

The frequency dynamics of the power system can be modeled using the swing equation and a differential equation representing the turbine-governor dynamics. The block diagram is shown in Fig. 2. The block diagram also contains a secondary power control loop, but the secondary control action is neglected because the main interest of this paper is the fast frequency dynamics. The following differential equations define the linearized frequency dynamics of the system:

$$M\Delta\dot{\omega} + D\Delta\omega = \Delta P_m - \Delta P_e \tag{6}$$

$$T_g\Delta\dot{P}_m + \Delta P_m = -R_p^{-1}\Delta\omega \tag{7}$$

where M represents the generator inertia constant, D represents the normalized damping constant, ω is the system frequency, P_m and P_e represent the mechanical power and electrical power, respectively, T_g represents the governor time constant, and R_p represents equivalent speed-regulation droop. Let us also define $x_\omega = [\Delta\omega\ \Delta\dot{\omega}]^\top$ as the states representing the system frequency dynamics and $u_\omega = \Delta P_e$ as the input. The state-space representation of the system frequency dynamics in SI units is thus given by:

$$\dot{x}_\omega = A_\omega x_\omega + B_\omega u_\omega \tag{8}$$

where

$$A_\omega = \begin{bmatrix} 0 & 1 \\ -\alpha & -\beta \end{bmatrix}; B_\omega = \begin{bmatrix} 0 \\ -\gamma \end{bmatrix}$$

$$\alpha = \frac{D}{MT_g} + \frac{1}{R_P MT_g}; \beta = \frac{D}{M} + \frac{1}{T_g}; \gamma = \frac{\omega_o}{S_b MT_g}$$

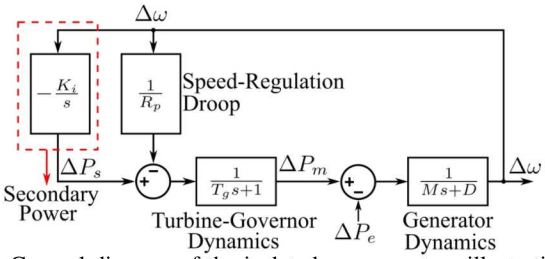

Fig. 2: General diagram of the isolated power system illustrating the generator dynamics and the primary frequency control loop.

In (8), the nominal power rating of the generator is S_b, while ω_0 is the nominal system frequency. The term $\Delta\dot{P}_e$ is neglected because $\Delta\dot{P}_e \ll \Delta P_e$ to simplify the model for the MPC implementation. This approximate model was shown to be effective in [8] to provide near-optimal fast-frequency support.

C. Integrated Voltage and Frequency Dynamics Model

In this section, we derive the integrated voltage and frequency dynamics model of the system by combining (3) and (8). Deriving these equations, the cross-coupling between the voltage and frequency dynamics is also illustrated. The set of differential equations for integrated voltage-frequency dynamics is given by:

$$\dot{\omega} = \dot{\omega} \tag{9}$$

$$\ddot{\omega} = -\alpha(\omega - \omega_o) - \beta\dot{\omega} - \frac{3}{2}\gamma(v_{gd}i_{gd} + v_{gq}i_{gq}) \tag{10}$$

$$\dot{i}_{gd} = -\frac{R}{L}i_{gd} + \omega i_{gq} + \frac{v_{cd}}{L} - \frac{v_{gd}}{L} \tag{11}$$

$$\dot{i}_{gq} = -\omega i_{gd} - \frac{R}{L}i_{gq} + \frac{v_{cq}}{L} - \frac{v_{gq}}{L} \tag{12}$$

$$\dot{v}_{cd} = -\frac{i_{gd}}{C} + \omega v_{cq} + \frac{i_{invd}}{C} - \frac{i_{Ld}}{C} \tag{13}$$

$$\dot{v}_{cq} = -\frac{i_{gq}}{C} - \omega v_{cd} + \frac{i_{invq}}{C} - \frac{i_{Lq}}{C} \tag{14}$$

In the derived model, we can see that there are several terms containing the product of ω and current/voltage. These terms reflect the coupling between voltage and frequency dynamics of the system. The above equations can be written in concise form as:

$$\dot{x} = f(x, u) \tag{15}$$

where $x = [\omega\ \dot{\omega}\ i_{gd}\ i_{gq}\ v_{cd}\ v_{cq}]^\top$ (state vector) and $u = [v_{gd}\ v_{gq}\ i_{invd}\ i_{invq}]^\top$ (input vector). Eq. (15) can be converted to discrete form as:

$$x_{k+1} = g(x_k, u_k) \tag{16}$$

D. Multi-timescale Dynamics

The time constants of all dynamics must be considered when selecting the sample time and horizon length of the MPC. The voltage and frequency dynamics in a microgrid system have different time constants. Ideally, for an computationally efficient controller, a multi-timescale control system would be adopted. However, this is beyond the scope of this paper and the same sampling rate is employed for both voltage and frequency control. The time constants of the voltage and frequency dynamics of the system are computed based on the eigenvalues of the corresponding system matrices.

1) Time Constant of Voltage Dynamics: To compute the time constant for the system's voltage dynamics, consider eigenvalues of the system matrix A_v as:

$$eig(A_v) = -\frac{R}{2L} \pm \frac{\sqrt{R^2 - \frac{4L}{C} - 4\omega^2L^2 \pm 4\omega L\sqrt{\frac{4L}{C} - R^2}}}{2L} \tag{17}$$

Generally, $\frac{4L}{C} \gg R^2$, and thus the voltage dynamics time constant can be estimated by:

$$T_v = \frac{2L}{R} \tag{18}$$

2) Time Constant of Frequency Dynamics: Similarly, to compute the time constant of frequency dynamics, consider the eigenvalues of the system matrix A_ω as:

$$eig(A_\omega) = -\frac{D}{2M} - \frac{1}{2T_g} \pm \frac{\sqrt{D^2T_g^2 - 2MDT_g + M^2 - \frac{4MT_g}{R_p}}}{2MT_g} \tag{19}$$

The $\frac{4MT_g}{R_p}$ term within the square-root is much larger than the other terms, allowing us to approximate the frequency dynamics time constant by:

$$T_\omega = \frac{2MT_g}{M + DT_g} \tag{20}$$

III. Proposed MPC Approach

A. Transformation of State Differential Equations

The state vector x shown in (15) has six components, but not all of them can be directly measured. For instance, the grid current i_g cannot be measured directly because the load in the real system is distributed. Instead, i_g can be estimated based on the measurement of i and v_c. Similarly, v_g cannot be directly measured. Thus, (9)–(14) need to be transformed such that i_g is expressed in terms of i. From i and v_c, we can estimate all the required terms — see (22)–(26). Additionally, the secondary control loop has not been considered in the predictive model as its effect can reduced by estimating an extra term, P_d, in Eq. (10). This extra term compensates for the unmodeled power (secondary power, load, etc). Defining $i_g = i - i_L$, the transformed equation becomes:

$$\dot{\omega} = \dot{\omega} \tag{21}$$

$$\ddot{\omega} = -\alpha(\omega - \omega_o) - \beta\dot{\omega} - \frac{3}{2}\gamma(v_{cd}i_d + P_d) \tag{22}$$

$$\dot{i}_d = -\frac{R}{L}i_d + \omega i_q + \frac{v_{cd}}{L} - \frac{v_d}{L} \tag{23}$$

$$\dot{i}_q = -\omega i_d - \frac{R}{L}i_q + \frac{v_{cq}}{L} - \frac{v_q}{L} \tag{24}$$

$$\dot{v}_{cd} = -\frac{i_d}{C} + \omega v_{cq} + \frac{i_{invd}}{C} \tag{25}$$

$$\dot{v}_{cq} = -\frac{i_q}{C} - \omega v_{cd} + \frac{i_{invq}}{C} \tag{26}$$

where $v_d = v_{gd} + \omega L i_{Lq} - R i_{Ld} - L\frac{di_{Ld}}{dt}$ and $v_q = v_{gq} - \omega L i_{Ld} - R i_{Lq} - L\frac{di_{Lq}}{dt}$. In (22), the grid voltage v_{gd} has been replaced with voltage across the capacitor v_{cd}. Because v_c will be the reference for control design, v_{cq} can be set to zero. This makes $v_{gd}i_{gd} + v_{gq}i_{gq} = v_{cd}(i_d - i_{Ld}) = v_{cd}i_d - v_{cd}i_{Ld}$. This second term $-v_{cd}i_{Ld}$ and other mismatch (due to secondary power) are included in P_d. The terms that cannot be measured, i.e., v_d, v_q and P_d, are estimated. Estimation of these variables is outside the scope of this paper and no estimator has been used. For this paper, data from one sample instant ahead are used in the discrete equations and those terms are calculated. This approximation is valid if the measurement noise is low, otherwise estimators must be used.

B. MPC Formulation

Let N be the horizon length. The objective is to control the voltage at the PCC v_c, as well as the system frequency ω to be within acceptable values. We can choose the axes such that the d-axis aligns with v_c so that v_{cq} is zero. Then the objective of the controller is to limit changes in v_{cd} and ω using the control inputs i_{invd} and i_{invq}. Next, let us assume $\Gamma = \{1, 2, ..., N\}$ represents the discrete sample time instants in the forward-time horizon. Let $y_k = [\Delta\omega_k \ \Delta\dot{\omega}_k \ \Delta v_{cdk}]^\top$ be the measured output of the system at a discrete time instant k, where Δ represents deviation from its nominal value, and $u_k = [i_{invd_k} \ i_{invq_k}]^\top$ is the input. Then, the proposed MPC formulation will take the following form:

$$\begin{aligned} \underset{i_{invd}, i_{invq}}{min} \quad & J_\Gamma = \sum_{k=1}^{N} (y_k^\top Q y_k + u_k^\top S u_k) \\ \text{s.t.} \quad & x_{k+1} = g(x_k, u_k) \ \forall \ k \in \Gamma, \\ & |i_{invd_k}| \leq i_{d,max} \ \forall \ k \in \Gamma, \\ & |i_{invq_k}| \leq i_{q,max} \ \forall \ k \in \Gamma, \\ & |i_{invd_{k+1}} - i_{invd_k}| \leq S_d \ \forall \ k \in \Gamma, \\ & |i_{invq_{k+1}} - i_{invq_k}| \leq S_q \ \forall \ k \in \Gamma \end{aligned} \tag{27}$$

where $i_{d,max}$ and $i_{q,max}$ are the limit on d and q components of inverter current, respectively, and S_d and S_q are the ramp rate limits on i_{invd} and i_{invq}, respectively. The system dynamics are incorporated within the first constraint of the MPC formulation. J_Γ is the cost function to be minimized, and Q and S are the weighting matrices corresponding to the states to be controlled and the control input, respectively. Good quality-of-service may come at the cost of inverter power (both active and reactive power). The cost function is defined such that cost on the inverter power and the degradation of the transient performance is included in the formulation. Depending on the cost of the control effort and the desired transient performance, the weighting matrices Q and S can be tuned. The Q matrix can be used to penalize poor system performance (i.e., to penalize deviation of $\Delta\omega$, $\Delta\dot{\omega}$, and Δv_{cd}), while the S matrix can be used to penalize the control effort (i.e., power output from the inverter). The weighting matrix Q is a 3×3 matrix defined as $diag(q_{11}, q_{22}, q_{33})$. Similarly, S is a 2×2 matrix be defined as $diag(s_{11}, s_{22})$. Solving this optimization problem over the time horizon Γ results in the following solution $i^*_{invd} = \{i^*_{invd_1}, i^*_{invd_2}, ..., i^*_{invd_N}\}$ and $i^*_{invq} = \{i^*_{invq_1}, i^*_{invq_2}, ..., i^*_{invq_N}\}$, with the first term of these two sequences used as the control signal in the next sample instant. This gives following control law:

$$i_{invd} = i^*_{invd_1}, \ i_{invq} = i^*_{invq_1} \tag{28}$$

IV. Simulation Setup

The simulation studies were carried out in MATLAB/Simulink. The simulation setup used is illustrated in Fig. 3. The system considered is a $100\ kVA$, $208\ V$ microgrid system. A load is connected at the PCC so that load variations result in voltage and frequency deviations. Without the MPC, the system frequency returns back to the nominal value after a certain time (depending upon the value of M, D, and T_g) based on the primary and secondary frequency controllers. However, if the inertia constant M is low, the system may experience large deviations in $\Delta\omega$ and $\Delta\dot{\omega}$. When the MPC is implemented, the inverter supplies d-axis current during the transient so that frequency deviation is lower during the transient. Similarly, the inverter supplies the q-axis current to support voltage at PCC. The MPC calculates the value of inverter current (control actions) that minimizes the cost function. The model and design parameters used are summarized in Table I. Line parameters are based on the typical design criteria of the line. The generator parameters are based on [8].

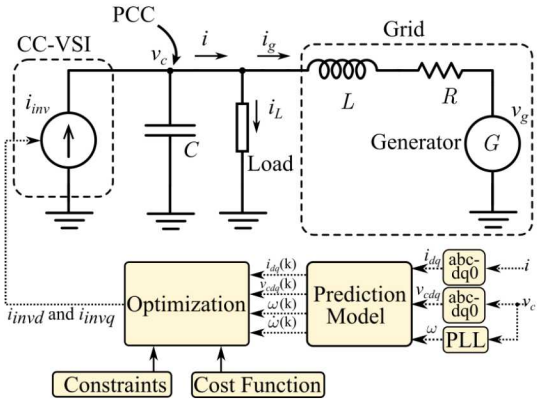

Fig. 3: Block diagram of the system with MPC

TABLE I: Summary of simulation parameters

Parameters	Values	Parameters	Values
R	0.08 Ω	T_g	0.2 s
L	0.22 mH	R_p	5 %
C	220 μF	Sample time (T_s)	0.4 ms
M	4 s	Horizon length (N)	1250
D	1.5		

Using the parameters Table I in (18), the voltage dynamics time constant is calculated as approximately $5\ ms$. As a rule of thumb, the controller sample time ($0.4\ ms$) was chosen to be approximately 15 times smaller than the voltage (lowest) time constant [10]. Similarly, the frequency dynamics time constant can be calculated based on (19). The controller horizon length of $0.5\ s$ is selected to be approximately 1.5 times the largest time constant, which in this case is 0.37 s for the frequency dynamics. It is important to note that for typical microgrid parameters, the voltage dynamics time constant is often much smaller than the frequency dynamics time constant.

Eq. (15) was discretized using the backward Euler method. A phase-locked-loop (PLL) was used to transform the capacitor voltage v_c and the current measurement i into the $dq0$ frame. The MPC was implemented in MATLAB/Simulink using CasADi, which is an open-source tool for non-linear optimization and algorithmic differentiation [11]. The optimization problem was formulated in C++ using CasADi and compiled to a Matlab Executable (MEX) file called from MATLAB/Simulink. The IPOPT nonlinear solver was employed to solve the optimization problem [12].

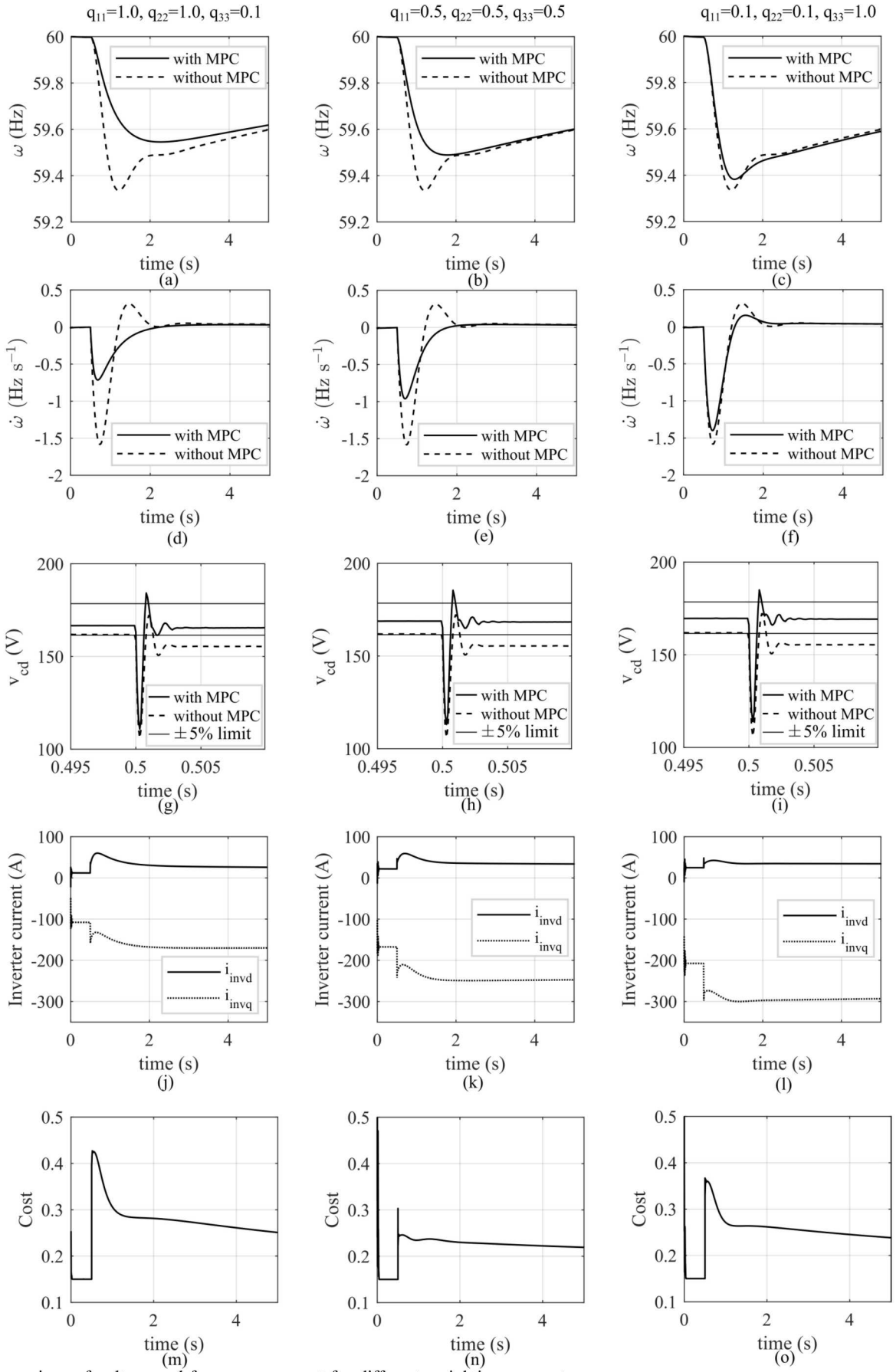

Fig. 4: Comparison of voltage and frequency support for different weighting parameters.

V. Results and Analysis

The proposed MPC for voltage and frequency support was simulated with different values of the weighting parameters. Three different cases were considered for the simulations through appropriate selection of the weighting matrices. In the first case, frequency support was prioritized over voltage support by setting $Q = diag(1.0, 1.0, 0.1)$. For the second case, equal emphasis was placed on voltage and frequency support by setting $Q = diag(0.5, 0.5, 0.5)$. The final case prioritized voltage support over frequency support by setting $Q = diag(0.1, 0.1, 1.0)$. For all cases, the values for s_{11} and s_{22} were chosen to be 0.01 and 0.001, respectively. This parameter selection assumes that voltage and frequency support has a higher priority over total energy cost. Among them, s_{11} is chosen ten times higher than s_{22} because active power is more expensive than reactive power. A step load change from 0.5 pu to 0.7 pu at $t = 0.5\ s$ is considered for all the cases to analyze the voltage and frequency dynamics of the considered system. Fig. 4 shows the simulation results for the three different cases.

TABLE II: Results summary

Performance Metrics	without MPC	Case I	Case II	Case III
Frequency nadir (Hz)	59.33	59.55	59.49	59.38
Maximum ROCOF (Hz s^{-1})	-1.57	-0.71	-0.96	-1.42
Time to nadir (s)	0.71	1.74	1.27	0.78
Voltage nadir (V)	106.24	110.81	113.19	114.31
Steady state voltage (V)	155.44	165.43	168.43	169.26

In the first case, significant reductions in the frequency deviation and rate of change of frequency (ROCOF) in Figs. 4(a) and (d) illustrate good frequency support has been achieved in the system. From Fig. 4(g), it can be observed that there is only a slight improvement in the voltage response. There is still a steady-state error on the voltage profile, although the error is within $\pm 5\%$. Fig. 4(j) shows the d- and q-axes inverter currents (control actions of the MPC). The initial spike is due to that fact that voltage dynamics are very fast, and thus large initial current is required to support the voltage transient. For frequency support, i_{invd} increases initially and as the secondary control loop reduces the frequency deviation, i_{invd} decreases. During steady-state, both i_{invd} and i_{invq} can provide voltage support. However, because a lower penalty is provided for the q-axis component (s_{11} is higher than s_{22}), i_{invq} regulates the voltage of the system during the steady-state. In the third case (which is the other extreme), voltage support is prioritized over frequency support. From Figs. 4(c) and (f), the frequency response is only slightly improved because a lower weight value is given to frequency support. Fig. 4(i) shows good improvement in the steady-state voltage response, returning back to the nominal value. In this case, a higher i_{invq} is observed because voltage support is given a higher priority, and hence more i_{invq} is required to reduce the cost function.

Finally, in the second case, weights have been selected such that priority is somewhere between the first and third cases. Here, both the frequency and voltage responses have slightly been improved. Table II provides a summary of how different system performance metrics such as frequency nadir, ROCOF, the time-to-nadir, voltage nadir, and steady-state voltage are affected by the selection of the weighting parameters.

VI. Conclusions

This paper presented a MPC framework to provide dynamic voltage and frequency support in microgrids. A model was derived to capture the cross-coupling between voltage and frequency dynamics. This model was employed in the proposed control framework. The controller maintained system frequency and voltage within limits for a representative microgrid with a large load transient. Furthermore, costs can be imposed on the inverter currents which allows the ESS operator to strike the right balance between voltage/frequency performance and ESS degradation.

VII. Acknowledgments

The author would like to thank Drs. Alvaro Furlani Bastos and Hyungjin Choi from Sandia National Laboratories for the technical review of this paper.

References

[1] F. Katiraei, R. Iravani, N. Hatziargyriou, and A. Dimeas, "Microgrids management," *IEEE power and energy magazine*, vol. 6, no. 3, pp. 54–65, 2008.

[2] G. Delille, L. Capely, D. Souque, and C. Ferrouillat, "Experimental validation of a novel approach to stabilize power system frequency by taking advantage of load voltage sensitivity," in *IEEE Eindhoven PowerTech*, 2015, 6 pp.

[3] M. Farrokhabadi, C. A. Cañizares, J. W. Simpson-Porco, E. Nasr, L. Fan, P. A. Mendoza-Araya, R. Tonkoski, U. Tamrakar, N. Hatziargyriou, D. Lagos *et al.*, "Microgrid stability definitions, analysis, and examples," *IEEE Transactions on Power Systems*, vol. 35, no. 1, pp. 13–29, 2019.

[4] K. W. Joung, T. Kim, and J. Park, "Decoupled frequency and voltage control for stand-alone microgrid with high renewable penetration," in *IEEE/IAS* 54^{th} *Industrial and Commercial Power Systems Technical Conference (ICPS)*, 2018, 8 pp.

[5] M. Ramezani and S. Li, "Voltage and frequency control of islanded microgrid based on combined direct current vector control and droop control," in *IEEE Power and Energy Society General Meeting (PESGM)*, 2016, 5 pp.

[6] M. Farrokhabadi, C. A. Cañizares, and K. Bhattacharya, "Frequency control in isolated/islanded microgrids through voltage regulation," *IEEE Transactions on Smart Grid*, vol. 8, no. 3, pp. 1185–1194, 2017.

[7] S. K. Sarkar, F. R. Badal, S. K. Das, and Y. Miao, "Discrete time model predictive controller design for voltage control of an islanded microgrid," in 3^{rd} *International Conference on Electrical Information and Communication Technology (EICT)*, 2017, 6 pp.

[8] U. Tamrakar, T. M. Hansen, R. Tonkoski, and D. A. Copp, "Model predictive frequency control of low inertia microgrids," in *2019 IEEE 28th International Symposium on Industrial Electronics (ISIE)*, 2019, pp. 2111–2116.

[9] Y. Shan, J. Hu, Z. Li, and J. M. Guerrero, "A model predictive control for renewable energy based AC microgrids without any PID regulators," *IEEE Transactions on Power Electronics*, vol. 33, no. 11, pp. 9122–9126, 2018.

[10] G. A. Perdikaris, *Discrete-Time Systems*. Dordrecht: Springer Netherlands, 1991, pp. 139–234. [Online]. Available: https://doi.org/10.1007/978-94-015-7929-2_3

[11] J. A. E. Andersson, J. Gillis, G. Horn, J. B. Rawlings, and M. Diehl, "CasADi – A software framework for nonlinear optimization and optimal control," *Mathematical Programming Computation*, vol. 11, no. 1, pp. 1–36, 2019.

[12] A. Wächter and L. T. Biegler, "On the implementation of an interior-point filter line-search algorithm for large-scale nonlinear programming," *Mathematical Programming*, vol. 106, no. 1, pp. 25–57, Mar 2006. [Online]. Available: https://doi.org/10.1007/s10107-004-0559-y